Temperature and concentration dependence of optical dephasing, spectral-hole lifetime, and anisotropic absorption in $Eu^{3+}:Y_2SiO_5$

Flurin Könz, Y. Sun, C. W. Thiel, and R. L. Cone
Department of Physics, Montana State University, Bozeman, Montana 59717, USA

R. W. Equall and R. L. Hutcheson
Scientific Materials Corporation, Bozeman, Montana 59715, USA

R. M. Macfarlane*
IBM Almaden Research Center, San Jose, California 95120, USA
(Received 4 April 2003; published 25 August 2003)

Detailed site-selective spectroscopy has been performed as a function of temperature on the $^7F_0 \leftrightarrow {}^5D_0$ transition of $Eu^{3+}:Y_2SiO_5$ for Eu^{3+} concentrations of 0.02%, 0.1%, 0.5%, and 1%. Time-domain optical dephasing, spectral hole lifetimes, anisotropic absorption coefficients, inhomogeneous linewidths, and fluorescence lifetimes for Eu^{3+} ions at both crystallographic sites were measured. The temperature dependence of the optical dephasing, transition energy, and linewidth of the $^7F_0 \rightarrow {}^5D_0$ absorption was measured and interpreted in terms of Raman scattering of phonons. Photon echo measurements of optical dephasing gave T_2 values as long as 2.6 ms, approaching the limit set by the fluorescence decay time. Spectral hole lifetimes were measured for temperatures from 2 K to 18 K, with observed lifetimes varying from 1 s at 18 K to an estimated value of greater than 20 days at 2 K. Anisotropic absorption coefficients were measured, and an increase in Eu^{3+} concentration from 0.02% to 7% produced an increase in the inhomogeneous linewidth Γ_{inh} from 0.5 GHz to ~150 GHz, indicating that Eu^{3+} doping induces significant strain in the crystal. New determinations of many energy levels of ^7F_J multiplets have been made for $J=0$ to 6.

DOI: 10.1103/PhysRevB.68.085109 PACS number(s): 42.50.Md, 78.40.−q, 42.62.Fi

I. INTRODUCTION

Excited-state dynamics, spin-lattice relaxation, inhomogeneous line broadening, and optical dephasing are some of the material properties that can be studied in detail using high-resolution coherent transient and hole-burning spectroscopies.[1] In addition, the ability to record spectral population gratings in an inhomogeneously broadened medium can be used to store and recall the spatial and spectral characteristics of laser pulse trains. This has led to applications for spectral-hole-burning materials in optical memories,[2–4] analog optical signal processing,[5,6] optical frequency references,[7] and laser spectral diagnostics. The material $Eu^{3+}:Y_2SiO_5$ is particularly attractive for these device applications because of its very long spectral-hole lifetimes and narrow homogeneous linewidths.[8,9] These same properties also make Eu^{3+} a sensitive probe for fundamental material studies of small environmental changes in the crystal.

Two of the most important parameters for optical data storage and processing using coherent transients or spectral hole burning are the inhomogeneous linewidth Γ_{inh} and the homogeneous linewidth Γ_h that is related to the dephasing time T_2 by $\Gamma_h = 1/(\pi T_2)$. The ratio Γ_{inh}/Γ_h is a measure of the maximum storage density enhancement achievable using the material's frequency selectivity. The optical dephasing time limits the duration of data pulse sequences in time-domain optical memories, while the inhomogeneous linewidth limits the spectral width of the data pulses and therefore the maximum achievable data rate. The spectral-hole lifetime is another important parameter, with applications existing for both long and short lifetimes. A large absorption coefficient for the optical transition is important for signal detection and generally depends on the concentration of the active ion; however, higher doping often introduces disorder and strain in the crystal so that the maximum absorption may not scale with concentration. In addition, high doping levels can give rise to spectral diffusion with a possible reduction in hole lifetime and an increase in the homogeneous linewidth.

The $Eu^{3+}:Y_2SiO_5$ material examined here has been studied by several groups[8–11] and exhibits one of the narrowest homogeneous optical transitions yet reported in a solid, $\Gamma_h = 122$ Hz, very close to the fluorescence lifetime limit of 81 Hz.[9] The hole-burning mechanism in $Eu^{3+}:Y_2SiO_5$ involves population storage in the ground state hyperfine levels, offering the potential for long storage times at low temperatures due to slow spin-lattice relaxation. Spectral holes burned by optical pumping of the Eu^{3+} hyperfine levels have lifetimes that we have extrapolated to more than 20 days at 2 K. In spite of the excellent characteristics of $Eu^{3+}:Y_2SiO_5$ for optical memories and processors, many spectroscopic properties critical for these applications, such as the strongly temperature dependent dephasing times and hole lifetimes, have not yet been reported. The study of these temperature dependences is the central focus of this paper. Measurements were performed on $Eu^{3+}:Y_2SiO_5$ crystals with Eu concentrations of 0.02%, 0.1%, 0.5%, 1%, and 7%.

The paper is organized as follows. Section II describes basic material properties of Y_2SiO_5. Section III details the spectroscopic properties. The $^7F_0 \rightarrow {}^5D_0$ anisotropic absorption, the $^5D_0$ fluorescence lifetimes, and the ^7F_J level structures, are discussed in Secs. III A, III B, and III C, respectively. Section IV describes the temperature dependences of

TABLE I. Concentration dependent peak absorption coefficients α_0 (cm^{-1}) and inhomogeneous linewidth Γ_{inh} (GHz) at $T=2$ K in $Eu^{3+}:Y_2SiO_5$. $D1$, $D2$, and b are the principal axes of the refractive index tensor. Γ_{inh} is the FWHM from the Lorentzian fit to the absorption line.

	α_0 (cm^{-1}) Site 1				α_0 (cm^{-1}) Site 2			
Eu^{3+} Conc.	$E\|D1$	$E\|D2$	$E\|b$	Γ_{inh} (GHz)	$E\|D1$	$E\|D2$	$E\|b$	Γ_{inh} (GHz)
0.02%	2.4	0.5	~0	0.63	1.1	0.2	1.2	0.50
0.1%	3.5	1.1	~0	1.7	1.7	0.3	2.2	1.4
0.5%	3.1	0.6	~0	11	1.3	0.2	1.3	12
1%	3.9	0.8	~0	22	1.2	0.3	1.5	32
7%	5.1			150	2.5			150

the transition energies and the linewidths. Finally, the temperature dependences of the spectral hole lifetimes are presented in Sec. V.

II. $Eu^{3+}:Y_2SiO_5$ MATERIAL PROPERTIES

The $^5D_0 \leftrightarrow {}^7F_0$ transition of Eu^{3+} is especially interesting since both the ground state $^7F_0$ and the excited state $^5D_0$ have $J=0$ and hence no first order electronic magnetic moment. This minimizes the sensitivity to spin flips in the crystalline environment, leading to very narrow homogeneous linewidths at low temperature. Low nuclear magnetic moment hosts may be chosen to further reduce dephasing due to nuclear spin flips.[12] In particular, Y_2SiO_5 is a good host since ^{89}Y has a nuclear spin of $I=\frac{1}{2}$ with a very small magnetic moment of $-0.137\mu_N$, ^{29}Si has an abundance of only 4.7% with a spin $I=\frac{1}{2}$ and a magnetic moment of -0.555 μ_N, and magnetic isotopes of oxygen have a negligible abundance of $<0.04\%$. Because magnetic interactions with the host lattice are minimized, this material exhibits subkilohertz homogeneous linewidths.[8,9] Additionally, the first $^7F_1$ excited state of Eu^{3+} is typically more than 200 cm^{-1} above the ground state, greatly reducing the magnitude of thermally induced line broadening and delaying its onset to higher temperatures.

The crystal host Y_2SiO_5 is monoclinic and belongs to the space group C_{2h}^6 with eight formula units in a unit cell. The cell parameters are[13] $a=1.041$ nm, $b=0.6721$ nm, $c=1.249$ nm, and $\beta=102°39'$. There are 1.83×10^{22} Y ions/cm^3 and Eu^{3+} ions substitute for Y^{3+} ions that occupy two crystallographically inequivalent sites of C_1 symmetry. Crystallographic axes (a, b, and c) were determined by Laue x-ray diffraction. The crystal is biaxial with the optical normal along the b axis and the other two principal axes ($D1$ and $D2$) in the $a-c$ plane. The orientation of $D1$ and $D2$ was determined by viewing the crystal between crossed polarizers; $D1$ is 23.8° from the c axis and 78.7° from the a axis and $D2$ is perpendicular to $D1$.[14] To measure the anisotropy of the optical properties, all investigated samples were oriented and the surfaces polished to optical quality. The dimensions of the crystals were chosen so that αL values at the peak of the absorption line were approximately 0.5 to minimize distortion in the measured line shapes and propagation effects in the photon echo experiments.

III. SPECTROSCOPIC PROPERTIES OF $Eu^{3+}:Y_2SiO_5$

A. Anisotropy of the $^7F_0 \rightarrow {}^5D_0$ absorption

Absorption experiments were carried out in a liquid helium cryostat operating either in bath or continuous gas-flow mode depending on the temperature required. For temperature dependent measurements, the crystals were attached to a copper sample holder with copper loaded grease. The temperature at the sample mount was measured with a calibrated carbon glass sensor (Lakeshore CGR-1-500).

The inhomogeneous linewidth of the $^7F_0 \leftrightarrow {}^5D_0$ transition for these samples varied from sub-GHz to 150 GHz as a function of concentration as shown in Table I. Linewidths narrower than 12 GHz (0.02% Eu, 0.1% Eu, and 0.5% Eu) were measured by laser absorption using a Coherent CR-599-21 single frequency cw dye laser. To minimize hole burning during the measurement, the laser beam was attenuated with neutral density filters and propagated through the crystal without focusing. Linewidths greater than 12 GHz (1%, 7% Eu) were measured by conventional absorption with a tungsten-halogen lamp. The crystal was masked to minimize scattered light in the background, and the transmitted light was analyzed using a SPEX 14018 spectrometer with a resolution of 3.5 GHz and a Hamamatsu R928 photomultiplier as the detector.

Absorption spectroscopy was performed for the two inequivalent sites with the electric vector of the light E parallel to $D1$, $D2$, and b at $T=2$ K and at room temperature. Typical results are shown in Fig. 1. At 2 K, the $^7F_0 \leftrightarrow {}^5D_0$ transition is at 17 240.2 cm^{-1} for site 1 and at 17 235.2 cm^{-1} for site 2, consistent with the measurements of previous authors.[8,9] Absorption was found to be anisotropic for both sites and the peak absorption coefficients and linewidths measured at 2 K are summarized in Table I for all samples studied. The peak absorption coefficient and the linewidth were obtained by fitting a Lorentzian line shape to the measured absorption profile. The strongest absorption for site 1 was found for $E\|D1$ and negligible absorption was found for $E\|b$. For site 2, absorption for $E\|D1$ and $E\|b$ is similar and both are greater than that for $E\|D2$.

The ionic radius mismatch between Eu^{3+} and Y^{3+} ions induces strain in the host lattice that contributes to the inhomogeneous broadening of optical transitions. Since increasing the dopant concentration increases the strain in the lattice, the inhomogeneous linewidth is expected to broaden for

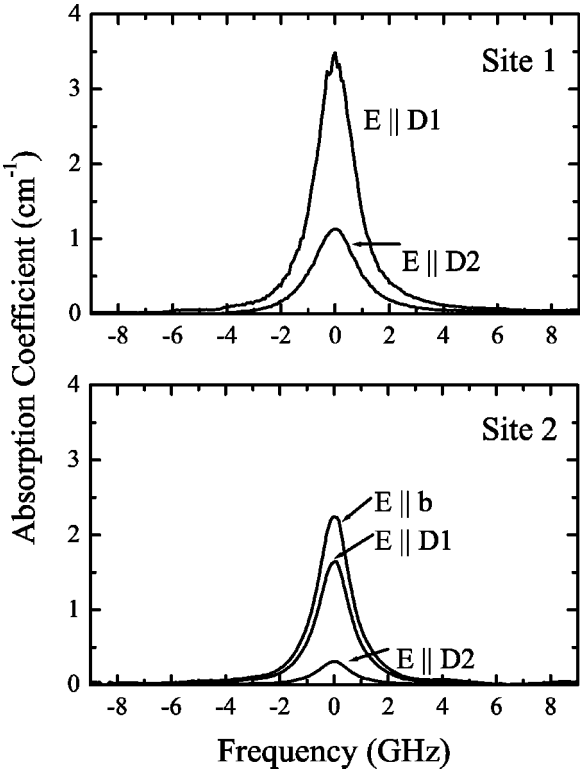

FIG. 1. Anisotropic absorption of the $^7F_0 \rightarrow {}^5D_0$ transition for 0.1% Eu^{3+}:Y_2SiO_5 at 2 K. The absorption coefficient of site 1 for $E \| b$ is ~ 0.

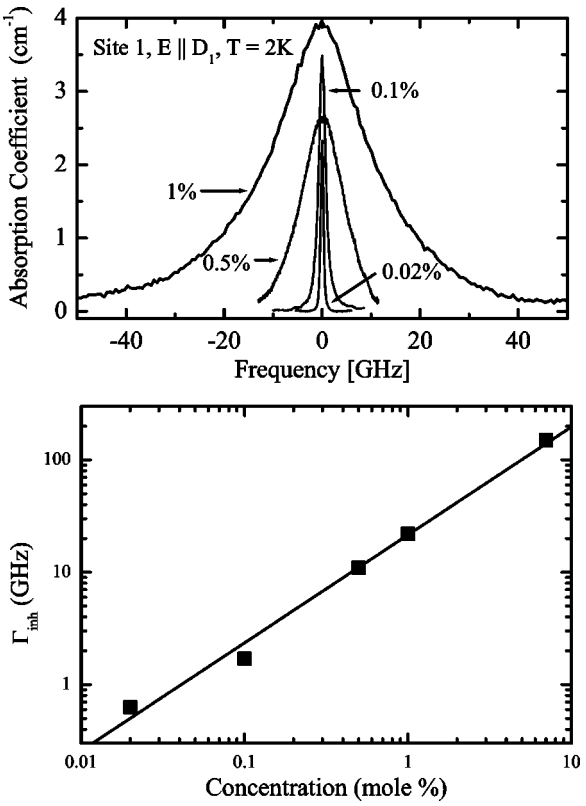

FIG. 2. Concentration dependence of the inhomogeneous linewidth for site 1. The upper plot shows the line shape data. Data for the 1% and 7% samples were measured with a spectrometer and a tungsten-halogen lamp. The resolution was 3.5 GHz. Data for the remaining samples were obtained using a single frequency laser with a resolution of ~ 1 MHz. The lower plot shows Γ_{inh} versus concentration. The slope is 21 GHz/unit concentration (in mole %).

higher concentrations. This trend was clearly observed in the measured inhomogeneous linewidths, as summarized in Table I and in Fig. 2, which shows a linear dependence of Γ_{inh} on Eu^{3+} concentration with a slope of 21 GHz/unit concentration (expressed in mole %). Lorentzian line shapes provided the best fit to the inhomogeneous absorption profile; that result is consistent with inhomogeneous broadening caused by Eu^{3+} point defects in the crystal.[15]

Since the inhomogeneous linewidth is proportional to the Eu^{3+} concentration, the peak absorption coefficients vary weakly with concentration as shown in Fig. 2. For the 0.1% sample, the highest absorption coefficient was measured to be 3.5 cm^{-1} for $E \| D1$ for site 1 and 2.2 cm^{-1} for $E \| b$ for site 2. With the assumption of equal site occupancy, the oscillator strength has the same value of 1.3×10^{-8} for site 1 and site 2. In this crystal, however, the two sites may not have equal occupancy, so the difference in absorption between the two sites could be a manifestation of a difference in the oscillator strengths, a difference in site occupancy, or both.

B. Fluorescence lifetime of $^5D_0$

The $^5D_0$ fluorescence lifetimes for both sites were measured by directly exciting the $^7F_0 \rightarrow {}^5D_0$ transition. The time-resolved fluorescence of the $^5D_0 \rightarrow {}^7F_2$ transition (16 376 cm^{-1} and 16 338 cm^{-1} for site 1 and 2, respectively) was detected using the spectrometer as a bandpass filter. The measurements were performed at both $T = 2$ K and room temperature. For experiments at $T = 2$ K, the laser was continuously scanned over 300 MHz so that spectral hole burning did not cause a significant reduction in the signal. The fluorescence lifetime T_1 of $^5D_0$ was measured for samples of each concentration, and the values are given in Table II. The measured fluorescence lifetime is slightly shorter at room temperature than at 2 K. At room temperature, there is a weak concentration dependence for site 1 and no concentration dependence for site 2.

C. Level structure of ^7F_J

The fluorescence spectra of $^5D_0 \rightarrow {}^7F_J$ were obtained by exciting $^5D_0$ directly. The fluorescence was analyzed using

TABLE II. Fluorescence lifetimes T_1 in milliseconds for both sites at 2 K and at 300 K.

Concentration	Site 1		Site 2	
	2 K	300 K	2 K	300 K
0.1%	1.97	1.82	1.62	1.57
0.5%	1.95	1.75	1.63	1.57
1.0%	1.94	1.69	1.62	1.57

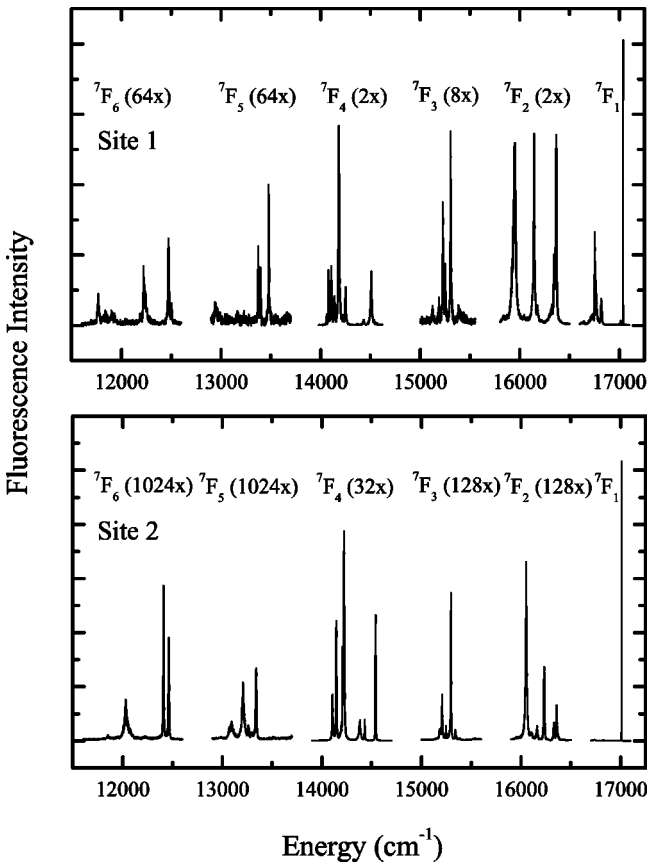

FIG. 3. Fluorescence spectra of $^5D_0 \rightarrow {}^7F_J$ for sites 1 and 2 of 1% Eu^{3+}:Y_2SiO_5. The numbers in parentheses indicate the scaling factors by which the data were expanded vertically for better visibility. The spectra were measured by exciting the $^5D_0$ level at 17 240.2 cm^{-1} for site 1 and 17 235.2 cm^{-1} for site 2. The spectra have not been corrected for the response of the spectrometer and detector.

the SPEX 14018 spectrometer and detected by photon counting using an RCA 31034A photomultiplier. The linewidths of the levels within the first 50 cm^{-1} of each J multiplet were measured by analyzing their fluorescence with an instrumental resolution of 0.2 cm^{-1} (6 GHz) which was much better than the minimum linewidth except for that of $^5D_0 \rightarrow {}^7F_1(1)$.

The fluorescence spectra from $^5D_0$ to all ^7F_J multiplets for both sites of the 1% Eu^{3+}:Y_2SiO_5 crystal are shown in Fig. 3. These spectra were used to determine the corresponding energies of the ^7F_J levels as summarized in Table III. Our measurements confirmed the $^7F_{1,2}$ level structure published in the literature[8] with the exception of the $^7F_1$ (3) and $^7F_2$ (3) levels of site 1 where small differences were noted. Since the local symmetry of the Eu^{3+} ion is C_1, none of the $^5D_0 \rightarrow {}^7F_J$ transitions are forbidden. For most of the multiplets with $J>3$, however, not all of the expected $2J+1$ lines were observed. The missing lines might be very weak, or they could be hidden under the envelope of other strong lines.

The linewidths of the transitions to ^7F_J levels are much broader than that of $^5D_0 \rightarrow {}^7F_0$ because of spontaneous phonon emission to the more closely spaced lower levels. The sharpest of these is the lowest component of $^7F_1$ whose width measured on the $^5D_0 \rightarrow {}^7F_1(1)$ transition of the 0.02% Eu sample was equal to the spectrometer resolution of 0.2 cm^{-1} (6 GHz). From this it is only possible to say that the combined homogeneous and inhomogeneous width of the transition is much less than 6 GHz, and higher resolution measurements are needed. The linewidths of the transitions from $^5D_0$ to the lowest component of all the other J manifolds are in the range of 5–11 cm^{-1} with the exception of that to the $^7F_4(1)$ of site 2, which is 2.5 cm^{-1}.

IV. TEMPERATURE DEPENDENCE OF THE $^7F_0 \leftrightarrow {}^5D_0$ TRANSITION ENERGY AND LINEWIDTH

Coupling between the electronic levels and thermally excited phonons results in temperature dependent line shifts and linewidths. The line shift is important in that it determines the thermal stability of data stored in the frequency domain or of frequency references obtained by locking lasers to spectral holes.[16] Thermally induced line broadening substantially reduces the optical coherence time at higher temperatures. The electron-phonon coupling in general is complicated by dependences of the coupling coefficients on both the branch and wave vector of the phonon modes, and by local modes due to the presence of the impurity. For direct or one-phonon processes, the phonon involved is resonant with an electronic level separation, in this case $^7F_1 - {}^7F_0$. For the

TABLE III. ^7F_J levels (cm^{-1}) measured at 2 K by fluorescence following excitation of the $^5D_0$ level in 1% Eu^{3+}:Y_2SiO_5 at 17 240.2 cm^{-1} for site 1 and 17 235.2 cm^{-1} for site 2.

Site 1						Site 2					
$^7F_1$	$^7F_2$	$^7F_3$	$^7F_4$	$^7F_5$	$^7F_6$	$^7F_1$	$^7F_2$	$^7F_3$	$^7F_4$	$^7F_5$	$^7F_6$
485	1283	2794	3183	4073	5472	493	1181	2054	3127	4161	5384
420	1086	2118	3160	4008	5403	407	1130	2026	3090	4146	5293
201	964	2050	3134	3958	5323	226	1077	1988	3045	4026	5204
	880	2012	3101	3865	5022		1002	1939	3025	3972	5015
	860	1987	3056	3842	4986		904	1893	3015	3940	4826
		1934	2991	3776	4830			1883	2855	3898	4773
		1848	2808	3759	4767				2804	3759	
			2732		4737				2737	3722	
			2676						2695		

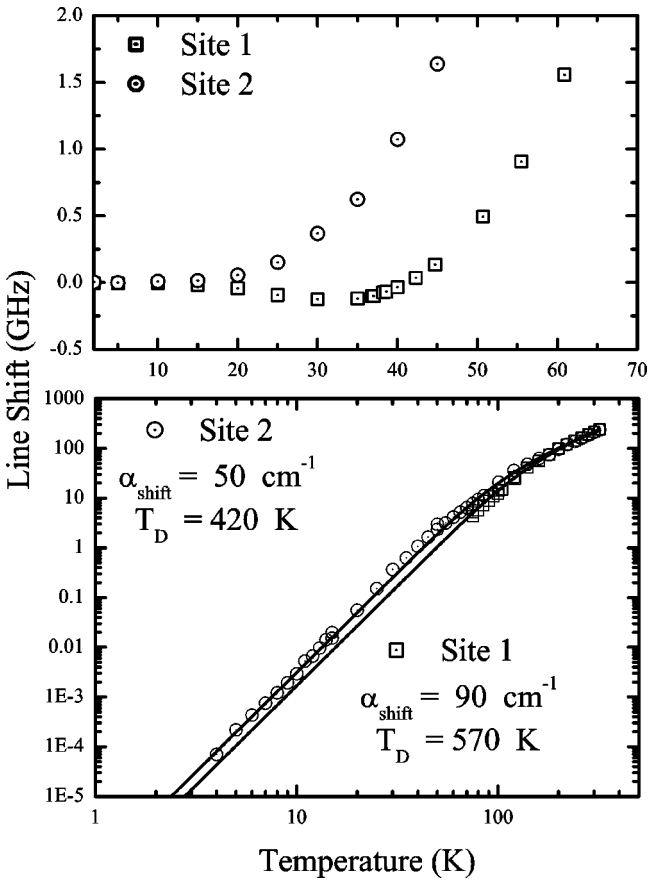

FIG. 4. Thermal line shift of the $^7F_0 \rightarrow {}^5D_0$ transition frequency. The upper graph shows the low temperature shift with the anomalous behavior for site 1. The lower graph shows the line shift from 4 K to 320 K for site 2 and over a smaller range for site 1 to avoid the region of the anomalous shift. The data were fit to a two-phonon Raman process of Eq. (1) with the resulting parameters shown.

two-phonon or Raman scattering term, the simplest approximation is to describe the interaction in terms of a single coupling coefficient to a Debye-type density of phonon states.[17] This description has two parameters, a coupling strength and an effective Debye temperature which sets the energy scale for the maximum phonon energy involved in the interaction. The effective phonon modes are those that are thermally occupied at a given temperature. The Debye temperature obtained from such a fit is not the same as that describing the heat capacity for example, since individual phonons will contribute differently in the two cases. As we shall see below, a fit to the linewidth over a large temperature range is difficult to make with a single coupling coefficient indicating the limitations of this simple model.

A. Line shifts

Figure 4 shows the thermally induced line shift of the $^7F_0 \rightarrow {}^5D_0$ transitions in the two sites at 17 240.2 cm^{-1} (site 1) and 17 235.2 cm^{-1} (site 2). Below 12 K, the shifts were measured from the shift of spectral holes burned in the absorption profile. From 12 K to 100 K, the position of the spectral line was measured by a scanned-laser absorption. From 100 K, to room temperature the absorption was measured with a spectrometer. It was found that the lines for both sites generally shift to higher frequencies as T increases, but the line for site 1 shows an anomalous shift to low energy below ~35 K (Fig. 4). Since the ground state is expected to shift to lower energy this overall behavior shows that the ground state shift is greater than the excited state shift as might be expected because the $^7F_1 - {}^7F_0$ energy difference is much smaller than that of $^5D_1 - {}^5D_0$.

The expression for the temperature dependent line shift due to the two-phonon Raman process is[17]

$$\Delta E(T) = \alpha_{\text{shift}} \left(\frac{T}{T_D} \right)^4 \int_0^{T_D/T} \frac{x^3\, dx}{e^x - 1}, \tag{1}$$

where $\Delta E(T)$ is the shift of the resonance line from its position in the absence of electron phonon coupling. Analytical expressions for the line shift can be obtained in the high temperature and low temperature limits. For these limiting cases we find that for high temperature,

$$\Delta E(T) = \frac{\alpha_{\text{shift}}}{3T_D} T - \frac{\alpha_{\text{shift}}}{8} \tag{2}$$

with less than 5% deviation from Eq. (1) for $T > 1.17 T_D$. For low temperature,

$$\Delta E(T) = \frac{\alpha_{\text{shift}} \pi^4}{15 T_D^4} T^4 \tag{3}$$

with less than 5% deviation from Eq. (1) for $T < 0.13 T_D$.

The experimental line shift data were fit to the expression of Eq. (1). For site 2 this yielded the parameters α_{shift} (site 2) $= 50 \pm 2$ cm^{-1} and an effective Debye temperature of $T_D = 420 \pm 10$ K. The overall shift for site 1 is very similar at higher temperatures and a fit to these data ignoring the anomalous behavior below ~70 K, gave α_{shift} (site 1) $= 90 \pm 4$ cm^{-1} and $T_D = 570 \pm 15$ K. The origin of the low temperature anomaly for site 1 is not understood at this time, but may involve a structural instability of the lattice.

B. Homogeneous linewidths

The homogeneous linewidth of the $^7F_0 \leftrightarrow {}^5D_0$ transition in $Eu^{3+}:Y_2SiO_5$ arises from three dominant mechanisms, namely $\Gamma_h = \Gamma_0 + \Gamma_{ISD} + \Gamma_{\text{phonon}}$. The ultimate limit for Γ_h is determined by the lifetime T_1 of the $^5D_0$ excited state, so $\Gamma_0 = 1/(2\pi T_1)$. This limit is 81 Hz for site 1 and 98 Hz for site 2. The contribution to the homogeneous linewidth due to excitation induced dephasing (instantaneous spectral diffusion) is described by Γ_{ISD}.[18–20] Excitation of ions during the echo sequence shifts the transition frequencies of neighboring ions, perturbs the phase relationships between the ions, and reduces the echo intensity. Thus, the echo signal decays faster, yielding a shorter effective T_2 and a broader Γ_h. For this reason, the specification of an optical dephasing time should be associated with a specific ion excitation density or preferably be extrapolated to zero excitation density. The Γ_{phonon} term describes the temperature dependence of the homogeneous linewidth due to coupling to phonons.

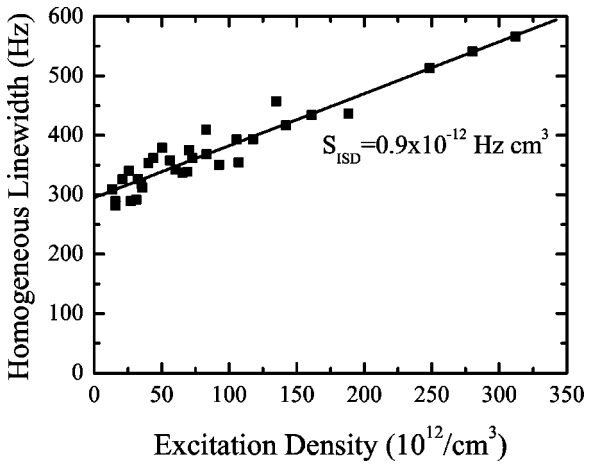

FIG. 5. Instantaneous spectral diffusion in the 1% sample using data obtained at four positions in the inhomogeneous line spaced 10 GHz apart.

At $T=2$ K, the homogeneous linewidth Γ_h in $Eu^{3+}:Y_2SiO_5$ is much smaller than the 1–2 MHz laser linewidth and the much broader inhomogeneous linewidths, requiring that measurements of Γ_h be made in the time domain by two-pulse photon echoes. Photon echo decays were found to be exponential, yielding the dephasing time T_2 that is related to Γ_h by $\Gamma_h=1/(\pi T_2)$. The excitation pulse sequence was generated by gating a single frequency dye laser with two acousto-optic modulators in series for improved contrast. Typical parameters were pulse durations between 0.5 and 2μs and laser intensities between 0.6 and 25 W/cm^2, resulting in pulse areas in the range $\pi/20$ to $\pi/4$. The shorter pulse lengths were chosen to reduce the effect of laser frequency jitter. The single longitudinal mode operation of the laser was monitored by a scanning Fabry–Perot etalon. The laser was continuously scanned over 300 MHz at ~120 MHz/s. This rate was chosen to be slow enough to ensure negligible hole burning during the photon echo experiments and fast enough to ensure spectral overlap of the exciting pulse pairs. The optical dephasing time was measured at several points in the absorption line and the corresponding absorption coefficient was noted. The repetition rate of the echo pulse sequences was 4 to 20 Hz. The laser frequency scan was not synchronized to the echo pulse sequences to minimize the contributions of stimulated echoes from spectral gratings burned by previous pulse sequences. Consecutive photon echo scans at a single spot in the crystal, and single echo decay measurements at different spots in the crystal, produced the same values for the optical dephasing times.

The homogeneous linewidth Γ_h was measured for several crystals as a function of concentration and excitation density. For the 1% sample, the homogeneous linewidth was also measured at four different positions in the inhomogeneous line profile separated by 10 GHz, and the results are plotted as a function of excitation density ρ_{ex} in Fig. 5. The excitation density ρ_{ex} is given by $3\times10^{12}I\tau\alpha$, with the echo excitation pulse width τ expressed in μs, the laser intensity I in W/cm^2, and the absorption coefficient α in cm^{-1}. When calculating the laser intensity I, we used the top-hat approximation for the area ($\frac{1}{2}\pi w_0^2$), where w_0 is the Gaussian beam waist.

When the homogeneous linewidth data are plotted as a function of laser intensity I, the presence of instantaneous spectral diffusion results in a slope $S(\alpha)$ that depends on the absorption coefficient.[9,11,20] Plotting the measured linewidth $\Gamma(I)$ as a function of excitation density (Fig. 5) normalizes these plots to a single line characterized by the material parameter $S_{\rm ISD}$ that describes the instantaneous spectral diffusion for a given material.[11] In this way we obtained $S_{\rm ISD}=0.9\times10^{-12}$ Hz cm^3 for all concentrations of $Eu^{3+}:Y_2SiO_5$. This result compares well with that of Graf *et al.*[11] (1.1×10^{-12} Hz cm^3), and acceptably with that of Equall *et al.*[9] (2×10^{-12} Hz cm^3), given the difficulty of determining absolute laser intensities. The homogeneous linewidth extrapolated to zero excitation density for the 0.02%, 0.1%, 0.5%, and 1% samples is 250±50 Hz. Equall *et al.* showed that applying a magnetic field of several hundred Gauss reduced this linewidth by ~100 Hz, an amount that was identified as a contribution from Y nuclear spin flips.[9] The ratio $\Gamma_{\rm inh}/\Gamma_h$ varies from 3×10^6 for the 0.02% sample to 9×10^7 for the 1% sample.

In general, $\Gamma_{\rm phonon}$ consists of both one-phonon or direct processes and two-phonon or Raman processes. For the one-phonon process, the strength of coupling can be determined from the spontaneous decay rate of $^7F_1(1)$. An upper bound on this can be obtained from the $^5D_0\rightarrow{}^7F_1(1)$ emission linewidth. From Sec. III C, we see that this is 6 GHz. Even taking this upper limit of 6 GHz for the coupling strength, the contribution to the linewidth from this term is at least an order of magnitude less than the observed width, so that it can be neglected. Contributions from the excited $^5D_0$ state are even smaller because of the larger $^5D_1$–$^5D_0$ separation. The contribution from the two-phonon Raman process is given by[17]

$$\Gamma_{\rm phonon}=\alpha_{\rm width}\left(\frac{T}{T_D}\right)^7\int_0^{T_D/T}\frac{x^6\,dx}{(e^x-1)^2}, \tag{4}$$

where $\alpha_{\rm width}$ is a coupling constant and T_D is the Debye temperature. We obtained an analytic expression for the linewidth expressed by Eq. (4) in the high and low temperature limits. At high temperatures,

$$\Gamma_{\rm phonon}=\frac{\alpha_{\rm width}}{5T_D^2}T^2-\frac{\alpha_{\rm width}}{84} \tag{5}$$

which is valid to better than 5% for $T>0.48T_D$, and at low temperatures, the integral changes very little for $T\ll T_D$ with

$$\Gamma_{\rm phonon}=\frac{\alpha_{\rm width}16\pi^6}{21T_D^7}T^7 \tag{6}$$

This expression is valid to better than 5% for $T<0.084T_D$.

The homogeneous linewidth was measured in the time domain for temperatures from 2 K to 12 K. Figure 6 shows examples of the normalized photon echo decays for site 1 of

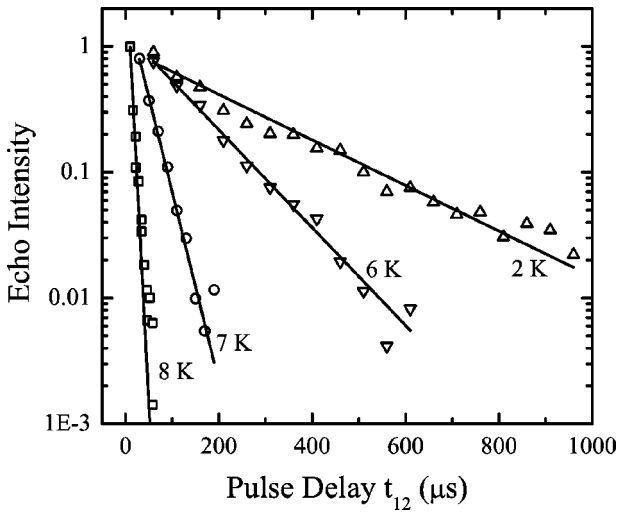

FIG. 6. Two-pulse photon echo decays measured in 0.1% Eu^{3+}:Y_2SiO_5 at different temperatures. The horizontal axis shows the delay time t_{12} between the two excitation pulses. With increasing temperature, the dephasing time T_2 shortens rapidly.

the 0.1% sample at four different temperatures. The dephasing time decreases dramatically with increasing temperature. Measurements were performed up to temperatures where the echo signal became comparable to the noise. At 10 K, we measured $\Gamma_h = 70$ kHz for site 1 and $\Gamma_h = 18$ kHz for site 2. The temperature dependence of the homogeneous linewidths obtained from photon echo measurements, $\Gamma_h(T)$-$\Gamma_h(0)$, is plotted on a logarithmic scale vs temperature in Fig. 7 for all measured Eu^{3+} concentrations and for both sites. The temperature dependence is close to T^7 as expected from the Raman mechanism, and we obtained coefficients of T^7 equal to 0.0072 Hz/K^7 for site 1 and 0.0018 Hz/K^7 for site 2. From these coefficients we find that $\alpha_{\text{width}}/T_D^7 = 9.8\times10^{-6}$ Hz/K^7 for site 1 and 2.5×10^{-6} Hz/K^7 for site 2. Over this limited temperature range, there is not enough information to separately determine α_{width} and T_D. Using the same Debye temperature for both sites results in a coupling coefficient for site 1 that is about 4 times larger than for site 2. For comparison with these results, we note that the coefficient of T^7 obtained by Babbitt *et al.*[21] for Eu^{3+}:Y_2O_3 was 0.0014, very similar to that found here for site 2.

To extend the homogeneous linewidth measurements to higher temperatures, we measured the total linewidth of the 0.1% sample by laser absorption. The temperature range covered in these measurements was from ~70 K, where the total linewidth was greater than the inhomogeneous linewidth, to ~100 K, where the width was too large for the 30 GHz laser scan. A third range was obtained by spectrometer measurements of the total linewidth of a 1% sample from ~180 K, where the width was larger than the spectrometer resolution, to 320 K. These two sets of data points, together with the low temperature set obtained from photon echoes, are shown for both sites on a logarithmic scale in Fig. 8. At room temperature, the total linewidth for the 1% sample is 3.1 cm^{-1} for site 1 and 2.3 cm^{-1} for site 2; i.e., about three times Γ_{inh}. For each site, the total $^7F_0 \rightarrow {}^5D_0$ absorption at room temperature is about 70% of that at 2 K due to reduction of the $^7F_0$ population by the thermal excitation of the low lying $^7F_1$ levels.

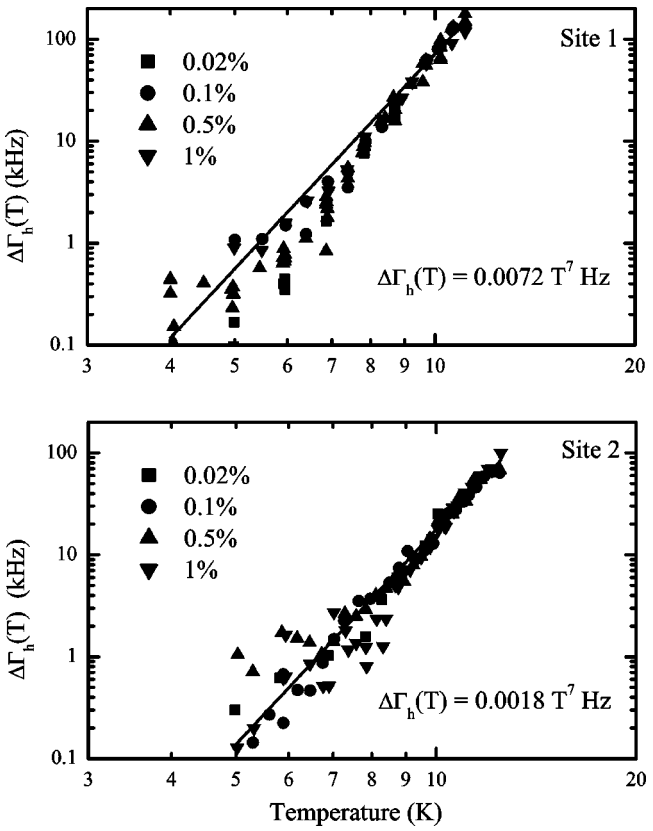

FIG. 7. Temperature dependent component of the homogeneous linewidth $\Delta\Gamma_h(T) = \Gamma_h(T) - \Gamma_h(0)$ vs absolute temperature for Eu^{3+}:Y_2SiO_5. The data for all measured Eu^{3+} concentrations and for both sites are included. The solid lines correspond to the theoretical model of two-phonon Raman scattering. The homogeneous linewidths for both site 1 and site 2 show a T^7 behavior, but the coupling between the phonons and electrons is weaker for site 2.

Analysis of the linewidth over this extended range of temperature with just the two parameters of the Raman process expressed by Eq. (4) does not result in a good fit. Certainly the nature of the phonons and the frequency dependence of the density of states appropriate for higher temperatures is very different from that of the acoustic phonons for the low temperature regime. We therefore made a fit with Eq. (4) for the intermediate and high temperature points and this is shown in Fig. 8. The resulting parameters are $T_D = 420$ K and $\alpha_{\text{width}}(\text{site 1}) = 27$ cm^{-1}, $\alpha_{\text{width}}(\text{site 2}) = 15$ cm^{-1}. This effective Debye temperature need not be closely related to the Debye temperature obtained from acoustic measurements, for example, because of the complex nature of the phonon density of states at the phonon energies that are thermally occupied near room temperature. Additional complexity arises from the possibility that near room temperature, direct process contributions from phonons resonant with the 400–500 cm^{-1} levels of $^7F_1$ may play a role. If we use this same Debye temperature of 420 K to describe the low temperature data, it implies a much higher coupling coefficient, as can be seen from Fig. 8.

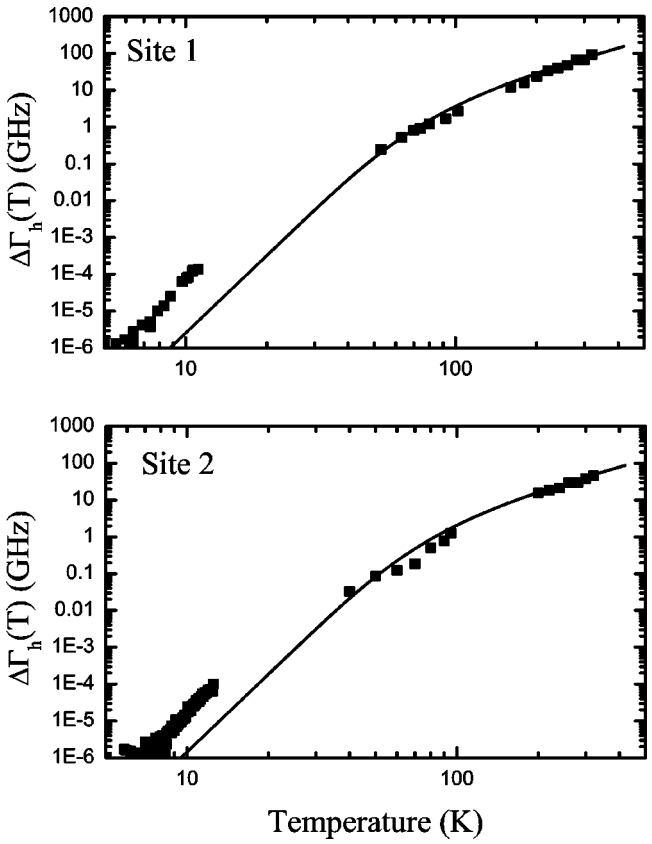

FIG. 8. Temperature dependent component of the homogeneous linewidth measured by photon echoes (low temperature), laser absorption (intermediate temperature), and tungsten-lamp absorption (high temperature). The solid line is a fit to Eq. (4) for the two-phonon Raman process for the intermediate and high temperature data.

V. SPECTRAL HOLE LIFETIME

Persistence of the spectral holes was measured by burning a hole at the center of the absorption line (10 $\mathrm{mW\,cm^{-2}}$ to 100 $\mathrm{mW\,cm^{-2}}$ for 2–4 s) and subsequently probing the spectral hole by scanning the laser with intensity attenuated by a factor of 10^3 to 10^4. The spectral holes were burned to depths of 50% to 90% of the absorption peak to ensure a good signal to noise ratio and the lifetime of the holes did not show any dependence on the hole depth. The experiments were repeated with half the original probing intensity to ensure that the probe beam did not influence the hole decay. Whenever practical, the decay was measured for an observation period corresponding to 4 times the lifetime and data points were taken for each temperature at intervals from 20 seconds to 10 minutes, depending on the lifetime. The area of the spectral hole, which is proportional to the stored population, was used for calculating the hole lifetime. The width of the observed spectral hole was limited by the laser frequency jitter of $\sim$2 MHz. For hole lifetimes shorter than 1 minute, the hole decay was measured by monitoring the transmission intensity of the weak probe laser without scanning.

The temperature dependence of the hole lifetime was measured from 2 K to 15 K for site 1, and from 10 K to 17 K for site 2, and is shown in Fig. 9. Data for crystals containing 0.02%, 0.1% and 1% Eu^{3+} are included and no dependence on concentration was found. In general, at any given temperature the hole lifetime of site 2 was about an order of magnitude longer than that of site 1, again indicating a weaker coupling of site 2 ions to the environment. A very large range of hole lifetimes was measured. For site 1, very long hole decays were measured at 2 K; data collected over 32 hours yielded a hole lifetime estimated to be 23 ± 5 days. Since the duration of the measurement was much shorter than the hole lifetime, the actual lifetime may be considerably longer. The hole lifetime of site 2 was not measured for temperatures lower than 10 K. The hole-burning mechanism in $Eu^{3+}:Y_2SiO_5$ is population redistribution among the ground-state hyperfine levels following optical pumping. There are two Eu isotopes, ^{153}Eu and ^{151}Eu, with roughly equal abundance. Both isotopes have a nuclear spin $I=\frac{5}{2}$. Since the ground state of Eu^{3+} is a singlet, the magnetic hyperfine interaction vanishes in first order. Therefore, the quadrupole interaction splits the hyperfine levels into three Kramers' doublets. The separation of the ground-state hyperfine levels was reported to be in the range of $\sim$100–300 MHz.[8] Multiexponential hole decays are expected, and observed, due to the different spin-lattice relaxation rates among the three hyperfine levels of each isotope. The hole lifetimes in Fig. 9 correspond to the 1/*e* point, so that they characterize the effective overall lifetime for the hole-burning process. Possible relaxation mechanisms include the direct one-phonon process, the two-step Orbach process,[22] and inelastic Raman scattering. The direct process, which involves the emission or absorption of a phonon, is very slow because of the low phonon density of states at the small hyperfine splitting frequencies. The Orbach process, in which a phonon is absorbed from $^7F_0$ to $^7F_1$ and subsequently re-emitted to a different hyperfine component of the ground state, is expected to show a temperature dependence

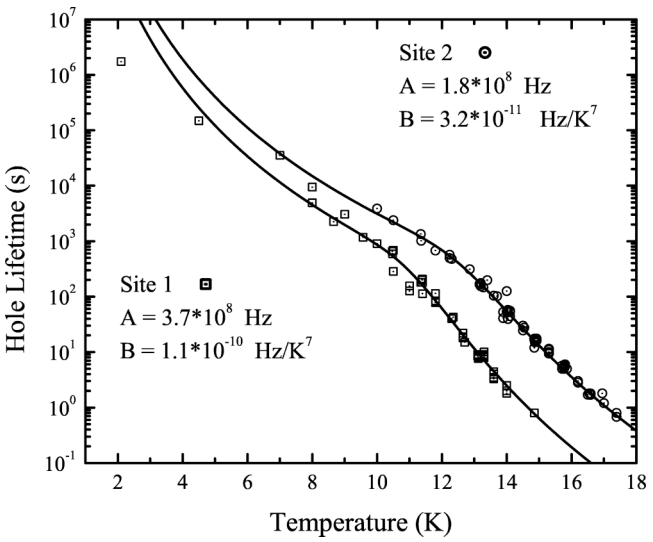

FIG. 9. Hole lifetime as a function of temperature for site 1 and site 2 showing a fit to the Raman and Orbach relaxation processes according to Eq. (7). The fit parameters are shown. The crossover from the Raman to the Orbach process occurs around 12 K.

given by the phonon occupation number $n(\delta E)$, where δE is the ${}^7F_0-{}^7F_1$ energy difference. The Raman process involves the inelastic scattering of phonons that exhibits a T^7 behavior at low temperature. The hole lifetime t_{hole} due to the Raman and Orbach processes can be written as

$$t_{\text{hole}}=\left[\frac{A}{e^{\delta E/kT}-1}+BT^7\right]^{-1} \tag{7}$$

in the low temperature regime, where A is the coefficient of the Orbach term and B of the Raman term. An initial fit of the hole lifetime to Eq. (7) gave values of δE within 5% of those measured from the fluorescence and given in Table III. This established the validity of the Orbach mechanism for the spin-lattice relaxation in this case. A final fit was then made fixing δE at the measured value and obtaining A and B as shown in Fig. 9. The Raman process dominates in the low temperature region below ~12 K and the Orbach process takes over above that. The two mechanism fit describes the overall temperature dependence of the hole lifetimes rather well. Spectral diffusion due to Eu–Eu interactions is not important, since the hole lifetime does not change with Eu^{3+} concentration.

VI. CONCLUSIONS

The absorption coefficients of the ${}^7F_0\rightarrow{}^5D_0$ transition in $Eu^{3+}:Y_2SiO_5$ crystals were measured at 2 K and at several temperatures up to room temperature. They are strongly polarization dependent, and the inhomogeneous linewidth broadens with increasing Eu^{3+} concentration, being ~0.5 GHz for 0.02% to 150 GHz for 7%.

The homogeneous linewidth was measured by two-pulse photon echoes. At the lowest temperatures (~2 K) the homogeneous linewidth is independent of Eu^{3+} concentration in the limit of zero excitation density. In the low temperature regime, the homogeneous linewidth shows a T^7 behavior due to a two-phonon Raman process. By 10 K the homogeneous linewidth broadens to 70 kHz for site 1 and 18 kHz for site 2 for all samples. An increase in concentration of Eu^{3+} ions to 1% does not produce any increase in Γ_h, but it does increase Γ_{inh} by a factor of 35 for site 1 and 64 for site 2. The ratio $\Gamma_{\text{inh}}/\Gamma_h$ is higher by these ratios in the 1% sample, i.e., $\sim 1\times 10^8$ for both sites. The lifetime of the spectral holes, which is a measure of the storage time of an optical hole-burning memory, depends strongly on the temperature. For site 1, the extrapolated decay times were found to be greater than 20 days at 2 K, 8 hours at 8 K, and 1 s at 15 K. For site 2, the lifetimes are even longer. The hole lifetime is independent of the Eu^{3+} concentration from 0.02% to 1%. Multiple components of the hole decay were observed due to the different spin-lattice relaxation rates between different hyperfine levels of the two Eu isotopes.

ACKNOWLEDGMENTS

Funding for this research was provided by the Swiss National Science Foundation, the Air Force Office of Scientific Research (AFOSR F49620-00-1-0314) and the National Science Foundation.

*Also at Department of Physics, Montana State University, Bozeman, MT 59717, USA.

[1] R.M. Macfarlane and R.M. Shelby, *Spectroscopy of Solids Containing Rare Earth Ions* (North-Holland, Amsterdam, 1987), pp. 51–184.

[2] T.W. Mossberg, Opt. Lett. **7**, 77 (1982).

[3] M. Mitsunaga, R. Yano, and N. Uesugi, Opt. Lett. **16**, 1890 (1991).

[4] T.W. Mossberg, Opt. Lett. **17**, 7 (1992).

[5] M. Zhu, W.R. Babbitt, and C.M. Jefferson, Opt. Lett. **20**, 2514 (1995).

[6] Z. Cole, T. Bottger, R.K. Mohan, R. Reibel, W.R. Babbitt, R.L. Cone, and K.D. Merkel, Appl. Phys. Lett. **81**, 3525 (2002).

[7] P.B. Sellin, N.M. Strickland, T. Bottger, J.L. Carlsten, and R.L. Cone, Phys. Rev. B **63**, 155111 (2001).

[8] R. Yano, M. Mitsunaga, and N. Uesugi, Opt. Lett. **16**, 1884 (1991).

[9] R.W. Equall, Y. Sun, R.L. Cone, and R.M. Macfarlane, Phys. Rev. Lett. **72**, 2179 (1994).

[10] G.J. Pryde, M.J. Sellars, and N.B. Manson, Phys. Rev. Lett. **84**, 1152 (2000).

[11] F.R. Graf, A. Renn, G. Zumofen, and U.P. Wild, Phys. Rev. B **58**, 5462 (1998).

[12] R.M. Macfarlane and R.M. Shelby, Opt. Commun. **39**, 169 (1981).

[13] B.A. Maksimov, V.V. Ilyukhin, Y.A. Kharitonov, and N.V. Belov, Sov. Phys. Crystallogr. **15**, 806 (1971).

[14] C. Li, C. Wyon, and R. Moncorgé, IEEE J. Quantum Electron. **28**, 3 (1992).

[15] A.M. Stoneham, Rev. Mod. Phys. **41**, 82 (1969).

[16] T Böttger, G.J. Pryde, and R.L. Cone, Opt. Lett. **28**, 200 (2003).

[17] D.E. McCumber and M.D. Sturge, J. Appl. Phys. **34**, 6 (1963).

[18] D.R. Taylor and J.P. Hessler, Phys. Lett. **50A**, 3 (1974).

[19] J. Huang, J.M. Zhang, A. Lezama, and T.W. Mossberg, Phys. Rev. Lett. **63**, 78 (1989).

[20] G.K. Liu and R.L. Cone, Phys. Rev. B **41**, 6193 (1990).

[21] W.R. Babbitt, A. Lezama, and T.W. Mossberg, Phys. Rev. B **39**, 1987 (1989).

[22] R. Orbach, Proc. R. Soc. London, Ser. A **264**, 458 (1961).